Supporting Information

Crystal Structure, Stability and Li Superionic Conductivity of Pyrochlore-Type Solid Electrolyte $Li_{2-x}La_{(1+x)/3}Nb_2O_6F$: A First-Principles Calculation Study

Randy Jalem,[1,*] Kazunori Takada,[1] Hitoshi Onodera[2], and Shuhei Yoshida[2]

[1]Center for Green Research on Energy and Environmental Materials (GREEN), National Institute for Materials Science (NIMS), 1-1 Namiki, Tsukuba, Ibaraki 305-0044, Japan

[2]Environment Neutral System Development Division, DENSO CORPORATION, 1 Yoshiike, Kusagi, Agui-cho, Chita-gun, Aichi 470-2298, Japan

Email: JALEM.Randy@nims.go.jp

Material synthesis

The $Li_{1.25}La_{0.58}Nb_2O_6F$ (LLNOF) solid electrolyte was prepared using the following synthesis conditions. Li_2CO_3, La_2O_3 and Nb_2O_5 reactant powders in stoichiometric ratio were calcined at 773 K and then heated at 1473 K for 6 hours to synthesize the precursor $Li_{0.5}La_{0.5}Nb_2O_6$. Next, the synthesized $Li_{0.5}La_{0.5}Nb_2O_6$ was mixed with LaF_3 and LiF. Here, 91%-excess LiF was added. The mixture was then heated at 1273 K for 6 hours to synthesize the target LLNOF powder.

Cyclic voltammetry measurement

The LLNOF electrolyte, acetylene black (AB) (conductive additive), and polyvinylidene fluoride (PVDF) (binder) were weighed in a mass ratio of 70:10:20 and then mixed with N-methyl-2-pyrrolidone (NMP) to form a paste. The paste was applied onto a copper foil and dried to make an electrode. The cyclic voltammetry evaluation was conducted using a 2032-type coin cell assembled with a Li anode. The electrolyte used was a solution of 1M $LiPF_6$ dissolved in a mixture of ethylene carbonate (EC) and dimethyl carbonate (DEC) in a volume ratio of 1:1. The coin cells were assembled in an Ar atmosphere inside a glove box. Cyclic voltammetry measurements were performed using a potentiostat/galvanostat device, with a scan voltage range of 0.02 V to 3V and a scan rate of 10 mV/s at 25°C.

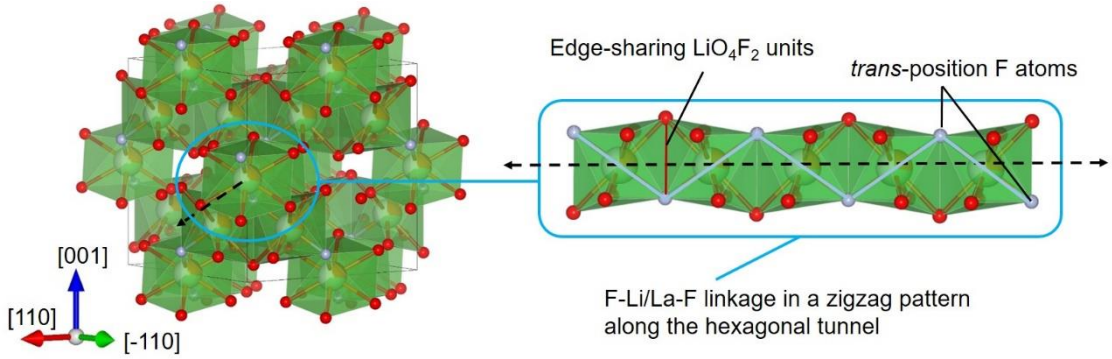

Figure S1. Visualization of the local structure of pyrochlore-type $Li_{2-x}La_{(1+x)/3}Nb_2O_6F$ (LLNOF) showing the F-Li/La-F linkage in a zigzag pattern along the characteristic hexagonal tunnel. The octahedral NbO_6 units are not displayed for clarity.

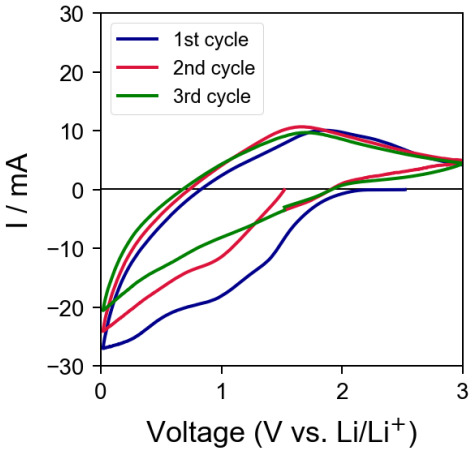

Figure S2. Cyclic voltammetry curves for the 1st, 2nd, and 3rd cycle of cell with LLNOF solid electrolyte.

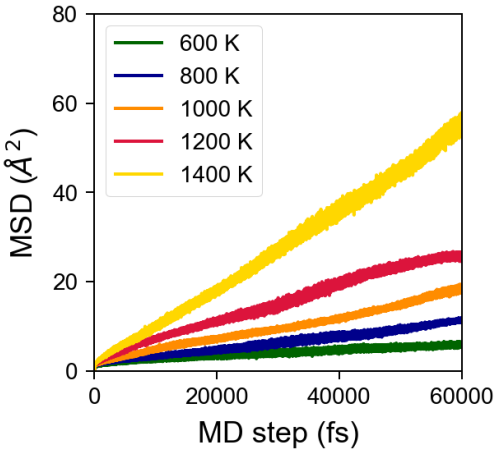

Figure S3. Mean squared displacement (MSD) plots for the Li atoms of pyrochlore-type $Li_{1.3125}La_{0.5625}Nb_2O_6F$ with the L1 structure (LLNOF-L1) from by NVT-AIMD calculations.

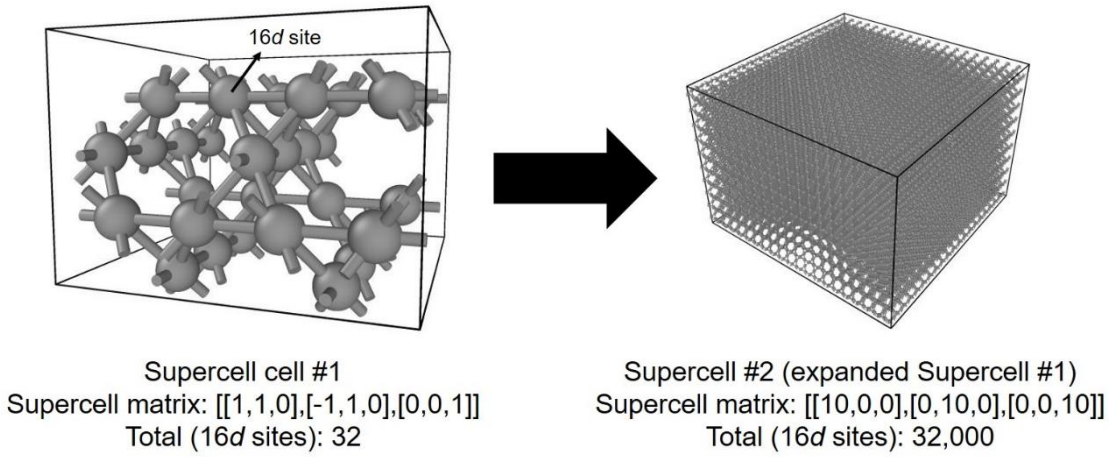

Figure S4. Supercell operation of the 16*d*-site cation sublattice in the $Li_{2-x}La_{(1+x)/3}Nb_2O_6F$ crystal structure for use in the calculation of Li^+ percolation threshold.

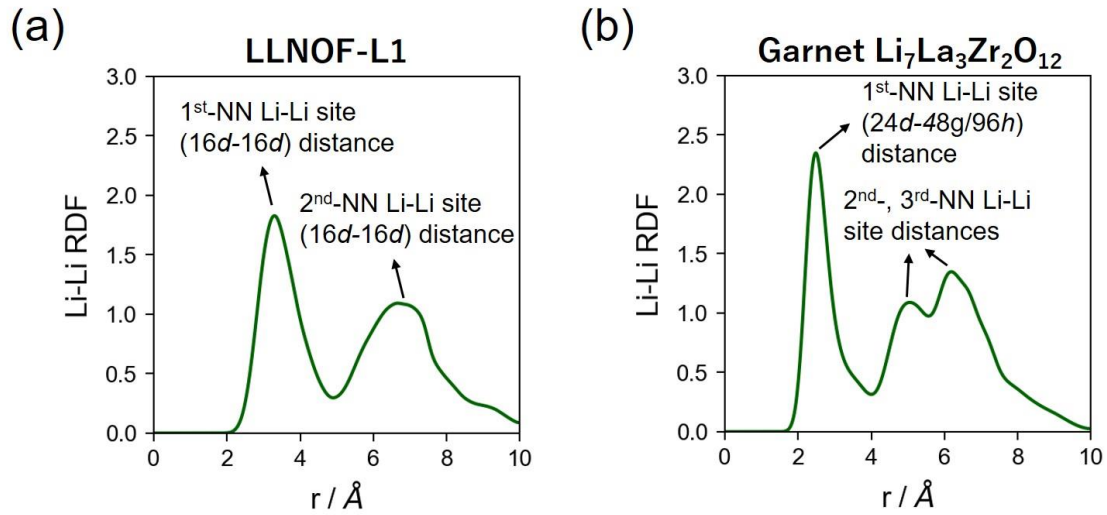

Figure S5. Li-Li radial distribution function (RDF) profiles derived from 1000-K NVT AIMD calculations for (a) pyrochlore-type $Li_{1.3125}La_{0.5625}Nb_2O_6F$ with the L1 structure (LLNOF-L1) and (b) garnet-type cubic $Li_7La_3Zr_2O_{12}$.

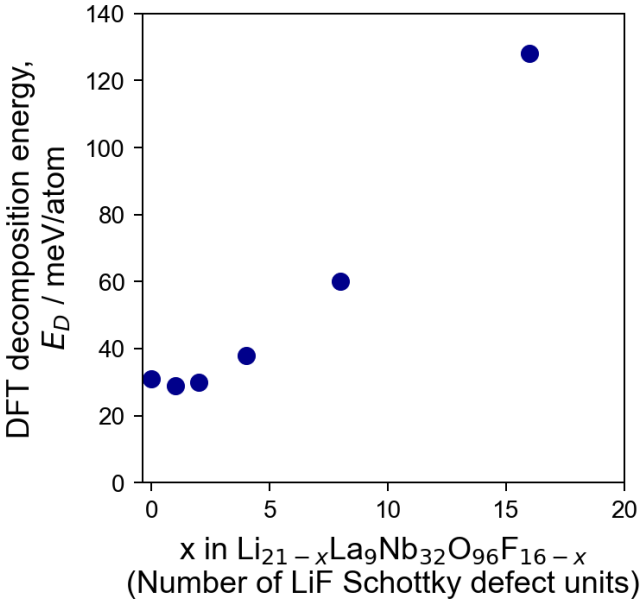

Figure S6. Plot for DFT decomposition energy as a function of the number of LiF Schottky defect units. The initial reference structure was based on $Li_{1.3125}La_{0.5625}Nb_2O_6F$ composition (L1 structure, supercell formula is $Li_{21}La_9Nb_{32}O_{96}F_{16}$ which is for x = 0).

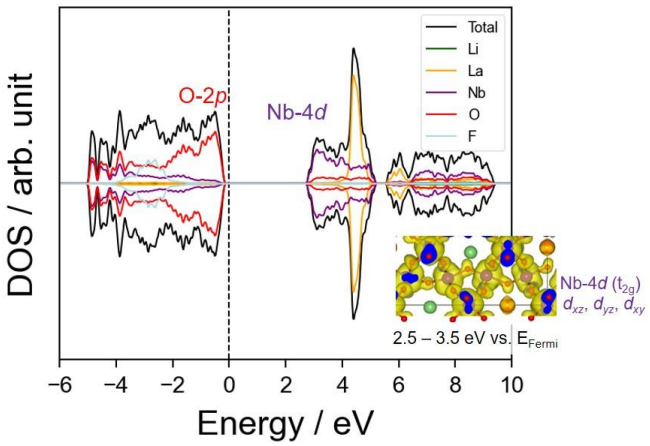

Figure S7. DFT-GGA electronic density of states (DOS) of pyrochlore-type $Li_{1.3125}La_{0.5625}Nb_2O_6F$ (LLNOF-L1 structure). The Fermi energy is referenced as zero in the horizontal axis.

Table S1. Crystal structure coordinate data of LLNOF by XRD Rietveld analysis, as reported in Ref. 12. Space group: $Fd\bar{3}m$ (cubic), lattice parameter a: 1.0445(1) nm, cell volume: 1.1396(1) nm^3.

Atom	Site	Occupancy (g)	Coordinates		
			x	y	z
La	16d	0.2771(6)	1/2	1/2	1.2
Li	16d	0.365(15)	x(La)	y(La)	z(La)
Nb	16c	1.0	0	0	0
O	48f	1.0	0.3151(2)	1/8	1/8
F	8b	0.989(8)	3/8	3/8	3/8

Table S2. Summary of DFT-predicted decomposition reactions related to the voltage stability window of pyrochlore-type $Li_{1.3125}La_{0.5625}Nb_2O_6F$ with the L1 structure (LLNOF-L1).

Voltage / V vs. Li/Li^+	Decomposition reaction
0 – 0.54	$Li_{21}La_9Nb_{32}(O_6F)_{16}$ + 160 Li → 4.5 La_2O_3 + 16 LiF + 82.5 Li_2O + 32 Nb
0.54 – 0.62	$Li_{21}La_9Nb_{32}(O_6F)_{16}$ + 64 Li → 4.5 La_2O_3 + 32 $LiNbO_2$ + 16 LiF + 18.5 Li_2O
0.62 – 0.96	$Li_{21}La_9Nb_{32}(O_6F)_{16}$ + 49.2 Li → 3.7 $Li_8Nb_2O_9$ + 4.5 La_2O_3 + 24.6 $LiNbO_2$ + 16 LiF
0.96 – 0.99	$Li_{21}La_9Nb_{32}(O_6F)_{16}$ + 45.5 Li → 4.5 La_2O_3 + 22.75 $LiNbO_2$ + 9.25 Li_3NbO_4 + 16 LiF
0.99 – 1.33	$Li_{21}La_9Nb_{32}(O_6F)_{16}$ + 41 Li → 20.5 $LiNbO_2$ + 11.5 Li_3NbO_4 + 7 LiF + 9 LaOF
1.33 – 1.74	$Li_{21}La_9Nb_{32}(O_6F)_{16}$ + 32 Li → 16 $LiNbO_2$ + 9 $LaNbO_4$ + 7 Li_3NbO_4 + 16 LiF
1.74 – 1.92	$Li_{21}La_9Nb_{32}(O_6F)_{16}$ + 18 Li → 14 $LiNbO_3$ + 9 $LiNbO_2$ + 9 $LaNbO_4$ + 16 LiF
1.92 – 2.35	$Li_{21}La_9Nb_{32}(O_6F)_{16}$ + 2.571 Li → 7.571 $LiNbO_3$ + 1.286 $Nb_{12}O_{29}$ + 9 $LaNbO_4$ + 16 LiF
2.35 – 2.49	$Li_{21}La_9Nb_{32}(O_6F)_{16}$ + 0.8889 Li → 5.889 $LiNb_3O_8$ + 0.4444 $Nb_{12}O_{29}$ + 9 $LaNbO_4$ + 16 LiF
2.49 – 3.92	$Li_{21}La_9Nb_{32}(O_6F)_{16}$ → 5 $LiNb_3O_8$ + 9 $LaNbO_4$ + 4 Nb_2O_5 + 16 LiF
3.92 – 3.93	$Li_{21}La_9Nb_{32}(O_6F)_{16}$ → 9 $LaNbO_4$ + 11.5 Nb_2O_5 + 16 LiF + 1.25 O_2 + 5 Li
3.93 –	$Li_{21}La_9Nb_{32}(O_6F)_{16}$ → 3.667 $LaNbO_4$ + 14.17 Nb_2O_5 + 5.333 LaF_3 + 5.25 O_2 + 21 Li

Table S3. Summary of DFT-predicted decomposition reactions related to the voltage stability window of $Li_3Nb_3O_8$ which is one of the decomposition phases of pyrochlore-type $Li_{1.3125}La_{0.5625}Nb_2O_6F$ with the L1 structure (LLNOF-L1).

Voltage / V vs. Li/Li^+	Decomposition reaction
0 – 0.54	4 $LiNb_3O_8$ + 60 Li → 32 Li_2O + 12 Nb
0.54 – 0.62	4 $LiNb_3O_8$ + 24 Li → 12 $LiNbO_2$ + 8 Li_2O
0.62 – 0.96	4 $LiNb_3O_8$ + 17.6 Li → 1.6 $Li_8Nb_2O_9$ + 8.8 $LiNbO_2$
0.96 – 1.74	4 $LiNb_3O_8$ + 16 Li → 4 Li_3NbO_4 + 8 $LiNbO_2$
1.74 – 1.92	4 $LiNb_3O_8$ + 8 Li → 8 $LiNbO_3$ + 4 $LiNbO_2$

1.92 – 2.35	4 $LiNb_3O_8$ + 1.143 Li → 5.143 $LiNbO_3$ + 0.5714 $Nb_{12}O_{29}$
2.35 – 3.92	4 $LiNb_3O_8$ → 4 $LiNb_3O_8$
3.92 –	4 $LiNb_3O_8$ → 6 Nb_2O_5 + O_2 + 4 Li

Table S4. Summary of DFT-predicted decomposition reactions related to the voltage stability window of LiF which is one of the decomposition phases of pyrochlore-type $Li_{1.3125}La_{0.5625}Nb_2O_6F$ with the L1 structure (LLNOF-L1).

Voltage / V vs. Li/Li^+	Decomposition reaction
0 – 6.36	LiF → LiF
6.36 –	LiF → 0.5 F_2 + Li

Table S5. Summary of DFT-predicted decomposition reactions related to the voltage stability window of $LaNbO_4$ which is one of the decomposition phases of pyrochlore-type $Li_{1.3125}La_{0.5625}Nb_2O_6F$ with the L1 structure (LLNOF-L1).

Voltage / V vs. Li/Li^+	Decomposition reaction
0 – 0.54	2 $LaNbO_4$ + 10 Li → 5 Li_2O + La_2O_3 + 2 Nb
0.54 – 0.62	2 $LaNbO_4$ + 4 Li → 2 $LiNbO_2$ + Li_2O + La_2O_3
0.62 – 0.96	2 $LaNbO_4$ + 3.2 Li → 1.6 $LiNbO_2$ + 0.2 $Li_8Nb_2O_9$ + La_2O_3
0.96 – 1.06	2 $LaNbO_4$ + 3 Li → 0.5 Li_3NbO_4 + 1.5 $LiNbO_2$ + La_2O_3
1.06 – 1.30	2 $LaNbO_4$ + 2 Li → 0.3333 Li_3NbO_4 + 0.6667 La_3NbO_7 + $LiNbO_2$
1.30 –	2 $LaNbO_4$ → 2 $LaNbO_4$

Table S6. Summary of DFT-predicted decomposition reactions related to the voltage stability window of Nb_2O_5 which is one of the decomposition phases of pyrochlore-type $Li_{1.3125}La_{0.5625}Nb_2O_6F$ with the L1 structure (LLNOF-L1).

Voltage / V vs. Li/Li^+	Decomposition reaction
0 – 0.54	14 Nb_2O_5 + 140 Li → 70 Li_2O + 28 Nb
0.54 – 0.62	14 Nb_2O_5 + 56 Li → 28 $LiNbO_2$ + 14 Li_2O
0.62 – 0.96	14 Nb_2O_5 + 44.8 Li → 2.8 $Li_8Nb_2O_9$ + 22.4 $LiNbO_2$
0.96 – 1.74	14 Nb_2O_5 + 42 Li → 7 Li_3NbO_4 + 21 $LiNbO_2$
1.74 – 1.92	14 Nb_2O_5 + 28 Li → 14 $LiNbO_3$ + 14 $LiNbO_2$
1.92 – 2.35	14 Nb_2O_5 + 4 Li → 4 $LiNbO_3$ + 2 $Nb_{12}O_{29}$

2.35 – 2.49	14 Nb_2O_5 + 3.111 Li → 3.111 $LiNb_3O_8$ + 1.556 $Nb_{12}O_{29}$
2.49 –	14 Nb_2O_5 → 14 Nb_2O_5

Table S7. Summary of DFT-predicted decomposition reactions related to the voltage stability window of garnet-type cubic $Li_7La_3Zr_2O_{12}$.

Voltage / V vs. Li/Li^+	Decomposition reaction
0 – 0.04	4 $Li_7La_3Zr_2O_{12}$ + 28 Li → 2 Zr_4O + 28 Li_2O + 6 La_2O_3
0.04 – 0.05	4 $Li_7La_3Zr_2O_{12}$ + 26.67 Li → 2.667 Zr_3O + 27.33 Li_2O + 6 La_2O_3
0.05 – 2.90	4 $Li_7La_3Zr_2O_{12}$ → 4 $Li_6Zr_2O_7$ + 2 Li_2O + 6 La_2O_3
2.90 – 3.16	4 $Li_7La_3Zr_2O_{12}$ → 4 $Li_6Zr_2O_7$ + Li_2O_2 + 6 La_2O_3 + 2 Li
3.16 – 3.24	4 $Li_7La_3Zr_2O_{12}$ → 7 Li_2O_2 + 4 $La_2Zr_2O_7$ + 2 La_2O_3 + 14 Li
3.24 – 3.72	4 $Li_7La_3Zr_2O_{12}$ → 1.75 LiO_8 + 4 $La_2Zr_2O_7$ + 2 La_2O_3 + 26.25 Li
3.72 –	4 $Li_7La_3Zr_2O_{12}$ → 4 $La_2Zr_2O_7$ + 2 La_2O_3 + 7 O_2 + 28 Li

Table S8. Summary of DFT-predicted decomposition reactions related to the voltage stability window of $Li_6Zr_2O_7$ which is one of the decomposition phases of garnet-type $Li_7La_3Zr_2O_{12}$ (LLZO).

Voltage / V vs. Li/Li^+	Decomposition reaction
0 – 0.04	2 $Li_6Zr_2O_7$ + 14 Li → Zr_4O + 13 Li_2O
0.04 – 0.05	2 $Li_6Zr_2O_7$ + 13.33 Li → 1.333 Zr_3O + 12.67 Li_2O
0.05 – 3.21	2 $Li_6Zr_2O_7$ → 2 $Li_6Zr_2O_7$
3.21 – 3.24	2 $Li_6Zr_2O_7$ → 4 Li_2ZrO_3 + Li_2O_2 + 2 Li
3.24 – 3.39	2 $Li_6Zr_2O_7$ → 4 Li_2ZrO_3 + 0.25 LiO_8 + 3.75 Li
3.39 – 3.72	2 $Li_6Zr_2O_7$ → 0.75 LiO_8 + 4 ZrO_2 + 11.25 Li
3.72 –	2 $Li_6Zr_2O_7$ → 4 ZrO_2 + 3 O_2 + 12 Li

Table S9. Summary of DFT-predicted decomposition reactions related to the voltage stability window of Li_2O which is one of the reductive decomposition phases of garnet-type $Li_7La_3Zr_2O_{12}$ (LLZO).

Voltage / V vs. Li/Li^+	Decomposition reaction
0 – 2.90	Li_2O → Li_2O
2.90 – 3.24	Li_2O → 0.5 Li_2O_2 + Li

3.24 – 3.72	$Li_2O \rightarrow 0.125\ LiO_8 + 1.875\ Li$
3.72 –	$Li_2O \rightarrow 0.5\ O_2 + 2\ Li$

Table S10. Summary of DFT-predicted decomposition reactions related to the voltage stability window of La_2O_3 which is one of the reductive decomposition phases of garnet-type $Li_7La_3Zr_2O_{12}$ (LLZO).

Voltage / V vs. Li/Li^+	Decomposition reaction
0 –	$La_2O_3 \rightarrow La_2O_3$

Table S11. Summary of DFT-predicted decomposition reactions related to the voltage stability window of garnet-type $Li_5La_3Ta_2O_{12}$ (LLTO).

Voltage / V vs. Li/Li^+	Decomposition reaction
0 – 0.35	$4\ Li_5La_3Ta_2O_{12} + 40\ Li \rightarrow 30\ Li_2O + 6\ La_2O_3 + 8\ Ta$
0.35 – 0.55	$4\ Li_5La_3Ta_2O_{12} + 10\ Li \rightarrow 6\ Li_5TaO_5 + 6\ La_2O_3 + 2\ Ta$
0.55 – 0.65	$4\ Li_5La_3Ta_2O_{12} + 2.5\ Li \rightarrow 7.5\ Li_3TaO_4 + 6\ La_2O_3 + 0.5\ Ta$
0.65 – 3.23	$4\ Li_5La_3Ta_2O_{12} \rightarrow 6.667\ Li_3TaO_4 + 1.333\ La_3TaO_7 + 4\ La_2O_3$
3.23 – 3.24	$4\ Li_5La_3Ta_2O_{12} \rightarrow 4\ La_3TaO_7 + 2\ Li_2O_2 + 4\ Li_3TaO_4 + 4\ Li$
3.24 – 3.47	$4\ Li_5La_3Ta_2O_{12} \rightarrow 0.5\ LiO_8 + 4\ La_3TaO_7 + 4\ Li_3TaO_4 + 7.5\ Li$
3.47 – 3.72	$4\ Li_5La_3Ta_2O_{12} \rightarrow 1.25\ LiO_8 + 2\ La_3TaO_7 + 6\ LaTaO_4 + 18.75\ Li$
3.72 –	$4\ Li_5La_3Ta_2O_{12} \rightarrow 2\ La_3TaO_7 + 6\ LaTaO_4 + 5\ O_2 + 20\ Li$

Table S12. Summary of DFT-predicted decomposition reactions related to the voltage stability window of Li_3TaO_4 which is one of the reductive decomposition phases of garnet-type $Li_5La_3Ta_2O_{12}$ (LLTO).

Voltage / V vs. Li/Li^+	Decomposition reaction
0 – 0.35	$Li_3TaO_4 + 5\ Li \rightarrow 4\ Li_2O + Ta$
0.35 – 0.55	$Li_3TaO_4 + Li \rightarrow 0.8\ Li_5TaO_5 + 0.2\ Ta$
0.55 – 3.59	$Li_3TaO_4 \rightarrow Li_3TaO_4$
3.59 – 3.72	$Li_3TaO_4 \rightarrow LiTaO_3 + 0.125\ LiO_8 + 1.875\ Li$
3.72 – 3.94	$Li_3TaO_4 \rightarrow LiTaO_3 + 0.5\ O_2 + 2\ Li$
3.94 – 4.03	$Li_3TaO_4 \rightarrow 0.3333\ LiTa_3O_8 + 0.6667\ O_2 + 2.667\ Li$

4.03 –	$Li_3TaO_4 \rightarrow 0.5\ Ta_2O_5 + 0.75\ O_2 + 3\ Li$

Table S13. Summary of DFT-predicted decomposition reactions related to the voltage stability window of Li_5TaO_5 which is one of the reductive decomposition phases of Li_3TaO_4.

Voltage / V vs. Li/Li^+	Decomposition reaction
0 – 0.35	$Li_5TaO_5 + 5\ Li \rightarrow 5\ Li_2O + Ta$
0.35 – 3.10	$Li_5TaO_5 \rightarrow Li_5TaO_5$
3.10 – 3.24	$Li_5TaO_5 \rightarrow 0.5\ Li_2O_2 + Li_3TaO_4 + Li$
3.24 – 3.59	$Li_5TaO_5 \rightarrow Li_3TaO_4 + 0.125\ LiO_8 + 1.875\ Li$
3.59 – 3.72	$Li_5TaO_5 \rightarrow LiTaO_3 + 0.25\ LiO_8 + 3.75\ Li$
3.72 – 3.94	$Li_5TaO_5 \rightarrow LiTaO_3 + O_2 + 4\ Li$
3.94 – 4.03	$Li_5TaO_5 \rightarrow 0.3333\ LiTa_3O_8 + 1.167\ O_2 + 4.667\ Li$
4.03 –	$Li_5TaO_5 \rightarrow 0.5\ Ta_2O_5 + 1.25\ O_2 + 5\ Li$

Table S14. Summary of DFT-predicted decomposition reactions related to the voltage stability window of La_3TaO_7 which is one of the reductive decomposition phases of Li_3TaO_4.

Voltage / V vs. Li/Li^+	Decomposition reaction
0 – 0.35	$La_3TaO_7 + 5\ Li \rightarrow 2.5\ Li_2O + 1.5\ La_2O_3 + Ta$
0.35 – 0.55	$La_3TaO_7 + 2.5\ Li \rightarrow 0.5\ Li_5TaO_5 + 1.5\ La_2O_3 + 0.5\ Ta$
0.55 – 0.65	$La_3TaO_7 + 1.875\ Li \rightarrow 0.625\ Li_3TaO_4 + 1.5\ La_2O3 + 0.375\ Ta$
0.65 –	$La_3TaO_7 \rightarrow La_3TaO_7$